

Dual structure in the charge excitation spectrum of electron-doped cupratesMatías Bejas,¹ Hiroyuki Yamase,² and Andrés Greco¹¹*Facultad de Ciencias Exactas, Ingeniería y Agrimensura and Instituto de Física Rosario (UNR-CONICET), Av. Pellegrini 250, 2000 Rosario, Argentina*²*National Institute for Materials Science, Tsukuba 305-0047, Japan*

(Received 21 September 2017; revised manuscript received 29 November 2017; published 28 December 2017)

Motivated by the recent resonant x-ray scattering (RXS) and resonant inelastic x-ray scattering (RIXS) experiments for electron-doped cuprates, we study the charge excitation spectrum in a layered t - J model with the long-range Coulomb interaction. We show that the spectrum is not dominated by a specific type of charge excitations, but by different kinds of charge fluctuations, and is characterized by a dual structure in the energy space. Low-energy charge excitations correspond to various types of bond-charge fluctuations driven by the exchange term (J term), whereas high-energy charge excitations are due to usual on-site charge fluctuations and correspond to plasmon excitations above the particle-hole continuum. The interlayer coupling, which is frequently neglected in many theoretical studies, is particularly important to the high-energy charge excitations.

DOI: [10.1103/PhysRevB.96.214513](https://doi.org/10.1103/PhysRevB.96.214513)**I. INTRODUCTION**

The origin of the charge order (CO), originally observed in underdoped hole-doped cuprates (h-cuprates) [1–14], is an active topic in condensed matter physics. The recent x-ray experiments for electron-doped cuprates (e-cuprates) [15,16] push the field even further. A CO occurs in an intermediate doping region and has a modulation vector along the $(0,0)$ - $(\pi,0)$ direction. These features are very similar to those observed in h-cuprates and suggest a common origin. However, this may require more careful studies because several experiments indicate a large asymmetry between e- and h-cuprates. For instance, the superconducting critical temperature T_c is much lower in e-cuprates than h-cuprates, and the pseudogap is weak or negligible in e-cuprates [17]. The last fact makes, in principle, e-cuprates simpler for a study of charge excitations because the CO may be formed from a homogeneous paramagnetic state and not from the pseudogap phase as in h-cuprates.

The charge excitation spectrum can be observed by resonant inelastic x-ray scattering (RIXS). The energy resolution of RIXS is presently about 50–100 meV and low-energy excitations are not sharply resolved compared with the high-energy ones. Given that the CO phenomena are associated with low-energy charge excitations, a natural question may arise: are the high-energy charge excitations observed by RIXS related to the low-energy charge excitations possibly associated with the CO?

This question can be studied for e-cuprates, where both the CO [15,16] and high-energy charge excitations [18,19] are observed in the same system. The CO was discussed in terms of resonant x-ray scattering (RXS). RXS measures the equal-time correlation function, that is, the spectral weight is integrated up to infinity with respect to energy. Thus, RXS cannot easily distinguish between a static order and a short-range fluctuating order. References [15,16] reported a short-range CO with a modulation vector $\mathbf{q}_{\parallel} \approx (0.5\pi, 0)$; here \mathbf{q}_{\parallel} denotes in-plane momentum. In contrast to the case in h-cuprates [20–26], the CO in e-cuprates has been studied only in a few theories [27,28]. In Ref. [27] it was discussed that the observed short-range CO is a d -wave bond order and its

modulation vector is determined by $2k_F$ scattering processes that connect the two Fermi momenta on the boundary of the Brillouin zone (BZ). The d -wave bond order is also proposed in Ref. [28] by employing a model different from that in Ref. [27]. On the other hand, high-energy spectrum revealed a quasilinear dispersive mode around $\mathbf{q}_{\parallel} = (0,0)$ with an energy gap about 300 meV [18]. The origin of this mode is under debate [18,19,29,30], and its relation with the CO phenomena is an open issue. A theoretical study of a layered t - J - V model [29] implies that this mode can be plasmons with a finite out-of-plane momentum q_z and originates from the usual on-site charge excitations.

From previous studies [27–29], it seems that the low-energy CO physics and the high-energy charge excitations are of different nature in e-cuprates. However, more work would be necessary before reaching such a conclusion. First, the CO was studied in the two-dimensional (2D) t - J model [27,31], whereas the high-energy mode was analyzed in the layered t - J - V model [29], with V being the long-range Coulomb interaction. Thus, it is not clear whether the obtained insight about the CO in the 2D t - J model remains valid also in a more realistic model such as the layered t - J - V model. Second, the CO was studied in Ref. [27] by focusing on a d -wave bond-order instability, which is a certain type of charge fluctuations. Possible contributions from other CO tendencies [31] were neglected. In particular, even if other CO tendencies are not leading, charge excitations associated with them could appear in a finite energy region. This possibility has never been studied. Third and most importantly, a global understanding of charge excitations has not been obtained in cuprates. If that is established in e-cuprates, it will certainly be an important step toward the understanding of charge excitations in h-cuprates. Therefore, it is a challenge to have a theory that may describe both low- and high-energy charge excitations on an equal footing and elucidate the charge excitation spectrum in a wide range of energy and momentum.

In this paper we study the momentum and energy resolved charge excitation spectrum of a layered t - J - V model in large- N expansion. The large- N analysis provides a nonperturbative scheme where all possible charge channels allowed

by symmetry can be handled on an equal footing, that is, a certain specific charge channel is not considered favorably by hand. This feature is particularly important to the present work because it is not clear what kinds of charge excitations are actually detected in x-ray experiments.

We find that various types of charge fluctuations contribute to the charge excitation spectrum, which is characterized by a dual structure in the energy space. The spectrum in the low-energy region is triggered by the charge sector of the exchange interaction J and originates from various bond-charge fluctuations, which may lead to the observed CO features [15,16]. On the other hand, the spectrum in the high-energy region is dominated by usual on-site charge fluctuations and is distinct from the spectrum of the low-energy bond-charge fluctuations. In particular, it is dominated by plasmons with a finite momentum transfer along the z direction.

The present paper is organized as follows. We first summarize our theoretical scheme in Sec. II, and then present results for the charge excitations in a realistic layered t - J - V model in Sec. III, including a comparison with the standard 2D t - J - V model. Our obtained results are discussed in Sec. IV in light of experimental data and conclusions are given in Sec. V. Appendixes discuss the q_z dependence of charge excitations and an alternative definition of bond-charge susceptibility.

II. THEORETICAL SCHEME

Since high- T_c cuprate superconductors are doped Mott insulators, a minimal model is the 2D t - J model on a square lattice. However, as we discuss in the present paper, this minimal model is not sufficient to describe all features observed in the charge excitation spectrum of e-cuprates. Two additional effects, which are frequently neglected in many theoretical studies, are indispensable: weak interlayer coupling along the z direction and the long-range Coulomb interaction. Hence we study the t - J model on a square lattice by including interlayer hopping and the long-range Coulomb interaction:

$$H = - \sum_{i,j,\sigma} t_{ij} \tilde{c}_{i\sigma}^\dagger \tilde{c}_{j\sigma} + \sum_{\langle i,j \rangle} J_{ij} \left(\vec{S}_i \cdot \vec{S}_j - \frac{1}{4} n_i n_j \right) + \sum_{\langle i,j \rangle} V_{ij} n_i n_j, \quad (1)$$

where the sites i and j run over a three-dimensional lattice. The hopping t_{ij} takes a value t (t') between the first (second) nearest-neighbors sites on the square lattice. The hopping integral between layers is scaled by t_z and the electronic dispersion is specified later [see Eq. (8)]. $\langle i,j \rangle$ denotes a nearest-neighbor pair of sites, and we consider the exchange interaction only inside the plane, namely $J_{ij} = J$, because the exchange term between the planes (J_\perp) is much smaller than J [32]. V_{ij} is the long-range Coulomb interaction on the lattice and is given in momentum space by

$$V(\mathbf{q}) = \frac{V_c}{A(q_x, q_y) - \cos q_z}, \quad (2)$$

where $V_c = e^2 d(2\epsilon_\perp a^2)^{-1}$ and

$$A(q_x, q_y) = \frac{\tilde{\epsilon}}{(a/d)^2} (2 - \cos q_x - \cos q_y) + 1. \quad (3)$$

These expressions are easily obtained by solving the Poisson's equation on the square lattice [33]. Here $\tilde{\epsilon} = \epsilon_\parallel / \epsilon_\perp$, and ϵ_\parallel and ϵ_\perp are the dielectric constants parallel and perpendicular to the planes, respectively; e is the electric charge of electrons; a is the lattice spacing in the planes and the in-plane momentum $\mathbf{q}_\parallel = (q_x, q_y)$ is measured in units of a^{-1} ; similarly d is the distance between the planes and the out-of-plane momentum q_z is measured in units of d^{-1} . $\tilde{c}_{i\sigma}^\dagger$ ($\tilde{c}_{i\sigma}$) is the creation (annihilation) operator of electrons with spin σ ($\sigma = \downarrow, \uparrow$) in the Fock space without double occupancy. $n_i = \sum_\sigma \tilde{c}_{i\sigma}^\dagger \tilde{c}_{i\sigma}$ is the electron density operator and \vec{S}_i is the spin operator.

Since the Hamiltonian (1) is defined in the Fock space without double occupancy, its analysis is not straightforward. Here we employ a large- N technique in a path integral representation of the Hubbard X operators [34]. This formalism allows us to study all possible charge instabilities already at leading order [26]. Furthermore, their dynamics turns out to capture essential features of charge dynamics observed in electron-doped cuprates [27,29,31,35]. Details of the formalism are summarized in Ref. [26] in the case of the 2D t - J model. It is easily extended to the present layered model as actually done in Ref. [29]. Hence we present only the essential part of our formalism here.

In the path integral formalism, our model (1) can be written in terms of a six-component bosonic field

$$\delta X_i^a = (\delta R_i, \delta \lambda_i, r_i^x, r_i^y, A_i^x, A_i^y), \quad (4)$$

fermionic fields, and interactions between bosonic and fermionic fields [26]. δR_i describes on-site charge fluctuations because it comes from $X_i^{00} = N \frac{\delta}{2} (1 + \delta R_i)$, where X_i^{00} is the Hubbard operator associated with the number of holes at a site i ; δ is the doped carrier density; the factor N comes from the sum over the N fermionic channels after the extension of the spin index σ from 2 to N . $\delta \lambda_i$ describes fluctuations of the Lagrangian multiplier introduced to impose the nondouble occupancy at any site. r_i^x and r_i^y (A_i^x and A_i^y) are fluctuations of the real (imaginary) part of a bond field along the x and y direction, respectively. This bond field is a Hubbard-Stratonovich field to decouple the exchange interaction in the model (1) and is parametrized as $\Delta_i^{x(y)} = \Delta (1 + r_i^{x(y)} + i A_i^{x(y)})$, where Δ is the mean-field value of the bond field, which is determined self-consistently [26], and is proportional to J . Thus the bond-charge fluctuations naturally appear in the present model. After Fourier transformation, the quadratic term of δX^a defines a 6×6 bare bosonic propagator $D_{ab}^{(0)}(\mathbf{q}, i\omega_n)$, which is given by

$$[D_{ab}^{(0)}(\mathbf{q}, i\omega_n)]^{-1} = N \begin{pmatrix} \frac{\delta^2}{2} [V(\mathbf{q}) - J(\mathbf{q})] & \frac{\delta}{2} & 0 & 0 & 0 & 0 \\ \frac{\delta}{2} & 0 & 0 & 0 & 0 & 0 \\ 0 & 0 & \frac{4\Delta^2}{J} & 0 & 0 & 0 \\ 0 & 0 & 0 & \frac{4\Delta^2}{J} & 0 & 0 \\ 0 & 0 & 0 & 0 & \frac{4\Delta^2}{J} & 0 \\ 0 & 0 & 0 & 0 & 0 & \frac{4\Delta^2}{J} \end{pmatrix}, \quad (5)$$

where $J(\mathbf{q}) = \frac{J}{2} (\cos q_x + \cos q_y)$ and the matrix indices a and b run from 1 to 6; \mathbf{q} is a three-dimensional wave vector and

ω_n is a bosonic Matsubara frequency. This bare propagator $D_{ab}^{(0)}(\mathbf{q}, i\omega_n)$ corresponds to the bare charge susceptibilities.

At leading order, the bare susceptibilities are renormalized to be

$$D_{ab}^{-1}(\mathbf{q}, i\omega_n) = [D_{ab}^{(0)}(\mathbf{q}, i\omega_n)]^{-1} - \Pi_{ab}(\mathbf{q}, i\omega_n), \quad (6)$$

because of coupling to fermions. The functional forms of the interaction vertices can be easily read off from the path integral formalism (see Fig. 1 in Ref. [34]) and is given by the six-component vertex h_a ,

$$h_a(\mathbf{k}, \mathbf{q}, \nu) = \left\{ \frac{2\varepsilon_{\mathbf{k}-\mathbf{q}} + \nu + 2\mu}{2} + 2\Delta \left[\cos\left(k_x - \frac{q_x}{2}\right) \times \cos\left(\frac{q_x}{2}\right) + \cos\left(k_y - \frac{q_y}{2}\right) \cos\left(\frac{q_y}{2}\right) \right]; 1; \right. \\ \left. -2\Delta \cos\left(k_x - \frac{q_x}{2}\right); -2\Delta \cos\left(k_y - \frac{q_y}{2}\right); \right. \\ \left. \times 2\Delta \sin\left(k_x - \frac{q_x}{2}\right); 2\Delta \sin\left(k_y - \frac{q_y}{2}\right) \right\}. \quad (7)$$

The electronic dispersion $\varepsilon_{\mathbf{k}}$ is given by

$$\varepsilon_{\mathbf{k}} = \varepsilon_{\mathbf{k}}^{\parallel} + \varepsilon_{\mathbf{k}}^{\perp}, \quad (8)$$

where the in-plane dispersion $\varepsilon_{\mathbf{k}}^{\parallel}$ and the out-of-plane dispersion $\varepsilon_{\mathbf{k}}^{\perp}$ are given, respectively, by

$$\varepsilon_{\mathbf{k}}^{\parallel} = -2 \left(t \frac{\delta}{2} + \Delta \right) (\cos k_x + \cos k_y) \\ - 4t' \frac{\delta}{2} \cos k_x \cos k_y - \mu, \quad (9)$$

$$\varepsilon_{\mathbf{k}}^{\perp} = 2t_z \frac{\delta}{2} (\cos k_x - \cos k_y)^2 \cos k_z, \quad (10)$$

and μ is the chemical potential. Note that the bare hopping integrals t , t' , and t_z are renormalized by a factor $\delta/2$. This renormalization is a leading order correction due to the local constraint because the t - J model is defined in the Fock space without double occupancy at any site. Note that k_z and q_z dependencies enter only through $\varepsilon_{\mathbf{k}-\mathbf{q}}$ in the first column in Eq. (7), whereas the other columns contain only the in-plane momentum \mathbf{q}_{\parallel} . Using the vertices $h_a(\mathbf{k}, \mathbf{q}, \nu)$, the 6×6 bosonic self-energies are computed at leading order as

$$\Pi_{ab}(\mathbf{q}, i\omega_n) = -\frac{N}{N_s N_z} \sum_{\mathbf{k}} h_a(\mathbf{k}, \mathbf{q}, \varepsilon_{\mathbf{k}} - \varepsilon_{\mathbf{k}-\mathbf{q}}) \\ \times \frac{n_F(\varepsilon_{\mathbf{k}-\mathbf{q}}) - n_F(\varepsilon_{\mathbf{k}})}{i\omega_n - \varepsilon_{\mathbf{k}} + \varepsilon_{\mathbf{k}-\mathbf{q}}} h_b(\mathbf{k}, \mathbf{q}, \varepsilon_{\mathbf{k}} - \varepsilon_{\mathbf{k}-\mathbf{q}}) \\ - \delta_{a1} \delta_{b1} \frac{N}{N_s N_z} \sum_{\mathbf{k}} \frac{\varepsilon_{\mathbf{k}} - \varepsilon_{\mathbf{k}-\mathbf{q}}}{2} n_F(\varepsilon_{\mathbf{k}}), \quad (11)$$

where N_s and N_z are the total number of lattice sites on the square lattice and the number of layers along the z direction, respectively. Therefore by studying $D_{ab}(\mathbf{q}, i\omega_n)$ [Eq. (6)], we can elucidate all possible charge dynamics in the layered t - J model at leading order in the large- N expansion.

If $J = 0$, δX^a reduces to a two-component bosonic field $\delta X^a = (\delta R, \delta \lambda)$, that is, the bosonic propagator D_{ab} becomes a 2×2 matrix and only usual on-site charge fluctuations are

active. When J is finite, bond-charge fluctuations become active and a and b take values from 1 to 6. Thus, in principle, the mixing between on-site and bond charge fluctuations is expected for finite J . We then define three sectors of the 6×6 bosonic propagator D_{ab} : (a) A 2×2 sector for $a, b = 1, 2$ which contains usual on-site charge fluctuations, (b) a 4×4 sector or J sector for $a, b = 3-6$, and (c) a 2×4 sector where $a = 1, 2$ and b runs from 3 to 6, and a 4×2 sector with $a = 3-6$ and $b = 1, 2$.

Finally, we mention the connection between the present model and charge excitations in the actual CuO_2 plane. It is known that the t - J model is an effective model and each lattice site corresponds to a Cu atom in the CuO_2 plane. However, the t - J model is derived from the three-band Hubbard model in the strong coupling limit [36] and thus the effect of O atoms is implicitly considered. Thus, whereas the usual charge susceptibility describes charge fluctuations on each Cu site, the susceptibilities defined by the J sector account for charge fluctuations between Cu sites, i.e., on the O sites.

III. RESULTS

In the following, we focus on parameters appropriate for e-cuprates [29], $J/t = 0.3$, $t'/t = 0.30$, and $t_z/t = 0.1$. For cuprates, a bare t is usually assumed to be around $t = 500$ meV [37], but we assume $t = 1$ eV because t is scaled as $t \rightarrow t/N$ in the large- N expansion and $N = 2$ in the actual material. All quantities with the dimension of energy are measured in units of t . We take the number of layers as $N_z = 30$, which is large enough. Concerning the long-range Coulomb interaction [Eq. (2)], we choose $d/a = 1.5$ [38] ($a = 4$ Å), $\varepsilon_{\parallel} = 4\varepsilon_0$, and $\varepsilon_{\perp} = 2\varepsilon_0$, where ε_0 is the vacuum dielectric constant [39]. We set the temperature (T) to zero and compute the imaginary part of various charge susceptibilities after analytical continuation $i\omega_n \rightarrow \omega + i\Gamma$ in Eq. (6). Here $\Gamma (> 0)$ is infinitesimally small and we choose $\Gamma = 10^{-3}$ for a numerical convenience. Computation is performed mainly for doping $\delta = 0.15$ to make a direct comparison with recent experiments in the e-cuprates [15,16,18,19]. The temperature is $T = 0$. Since q_z is in general finite in RIXS, we will present results mainly for $q_z = \pi$ as representative ones.

We first study each element of $D_{ab}(\mathbf{q}, \omega)$ [Eq. (6)], which has not been clarified yet in the literature to the best of our knowledge. We then study usual on-site charge and bond-charge excitations, which are described by various combinations of the elements of $D_{ab}(\mathbf{q}, \omega)$. The superposition of these two kinds of charge excitations reveals a dual structure of the charge spectrum. We also present results of ω -integrated spectral weight because RIXS can measure it directly. Finally, we make a comparison with results in the standard 2D t - J - V model.

A. Elements of $D_{ab}(\mathbf{q}, \omega)$

In the present theoretical framework, all possible charge susceptibilities are described by various combinations of the elements in the 6×6 matrix $D_{ab}(\mathbf{q}, \omega)$. Therefore, we first study excitation spectra of each element of the matrix. In Fig. 1 we show \mathbf{q}_{\parallel} - ω maps of $\text{Im} D_{ab}(\mathbf{q}, \omega)$ along the symmetry axes

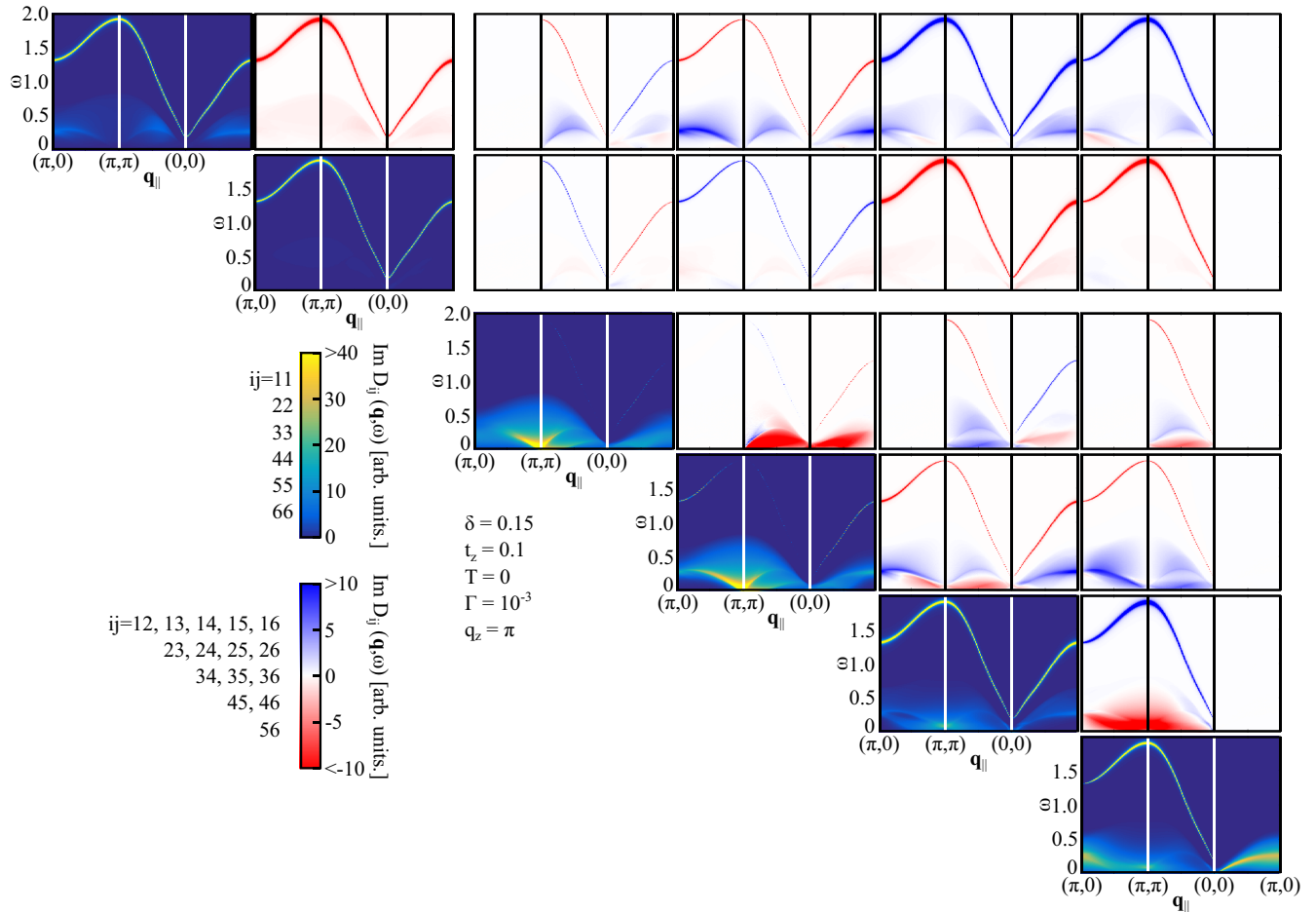


FIG. 1. \mathbf{q}_{\parallel} - ω maps of each element of $\text{Im}D_{ab}(\mathbf{q}, \omega)$ along the symmetry axes $(\pi, 0)$ - (π, π) - $(0, 0)$ - $(\pi, 0)$; the out-of-plane momentum is $q_z = \pi$. The elements are placed in a 6×6 matrix form and only the upper triangle of the matrix is shown because $D_{ab}(\mathbf{q}, \omega)$ is symmetric. To clarify each sector of 2×2 , 4×4 , and 2×4 , a small space is inserted between each sector.

for $q_z = \pi$. Since $D_{ab}(\mathbf{q}, \omega)$ is a symmetric matrix, we show only the upper triangle of the matrix.

All diagonal elements of $\text{Im}D_{ab}(\mathbf{q}, \omega)$ have positive spectral weight. We see two typical features: (i) a continuum spectrum at relatively low energy with a scale of $J (= 0.3)$ and (ii) a sharp mode extending from $\omega \approx 0.2$ at $\mathbf{q}_{\parallel} = (0, 0)$ to $\omega \approx 2.0$ at $\mathbf{q}_{\parallel} = (\pi, \pi)$. The former spectrum comes from particle-hole excitations and their spectral intensity in D_{11} and D_{22} is much weaker than in D_{33} , D_{44} , and D_{66} . In particular, the spectral weight of the continuum in D_{22} is almost invisible in the scale of Fig. 1. The sharp mode is realized above the particle-hole continuum and originates from the zeros of the determinant of $D_{ab}^{-1}(\mathbf{q}, \omega)$, i.e., it is a collective mode. Thus, this mode in principle can appear in all elements of $D_{ab}(\mathbf{q}, \omega)$. However, the mode vanishes completely along the $(\pi, 0)$ - (π, π) direction in D_{33} and along the $(0, 0)$ - $(\pi, 0)$ direction in D_{66} . This is because the determinant of $D_{ab}^{-1}(\mathbf{q}, \omega)$ does not affect D_{33} and D_{66} along those directions. This special feature is connected with the vanishing of the spectral weight along the $(\pi, 0)$ - (π, π) direction in D_{13} , D_{23} , D_{34} , D_{35} , D_{36} , and along the $(0, 0)$ - $(\pi, 0)$ direction in D_{a6} with $a = 1-5$ (see Fig. 1), which is traced back to the fact that the corresponding $\Pi_{ab}(\mathbf{q}, \omega)$ in Eq. (6) vanishes due to the symmetry of the vertex h_a [Eq. (7)].

The off-diagonal elements of $\text{Im}D_{ab}(\mathbf{q}, \omega)$ might seem odd because some of them exhibit *negative* spectral weight. Those, of course, do not have a direct physical meaning. As we will show explicitly, the physical susceptibilities are defined by some combinations of the elements of $D_{ab}(\mathbf{q}, \omega)$ and they have positive spectral weight. Similar to the diagonal part, the off-diagonal elements have two typical features: a continuum spectrum limited to a low-energy region and a collective mode above the continuum. This mode is the same as that in the diagonal elements, namely the zeros of the determinant of $D_{ab}^{-1}(\mathbf{q}, \omega)$. Another intriguing aspect of Fig. 1 is that the continuum spectrum of D_{2a} with $a = 1-6$ are typically very weak compared with others. D_{2a} contains $\delta\lambda$, which describes fluctuations of the Lagrangian multiplier imposing nondouble occupancy at any site. While the case of $q_z = \pi$ is plotted in Fig. 1, the q_z dependence is very weak and essentially the same results are obtained for different values of q_z except for $q_z \approx 0$ around $\mathbf{q}_{\parallel} = (0, 0)$; see Appendix A and also Ref. [29] where the element $(1, 1)$ of $D_{ab}(\mathbf{q}, \omega)$ is studied in detail.

The collective mode is nothing more than plasmons [29], which are driven by the 2×2 sector. In order to demonstrate this statement, we show in Fig. 2 the zeros of the determinant of $D_{ab}^{-1}(\mathbf{q}, \omega)$ for $J = 0.3$ and $J = 0$ along the symmetry axes.

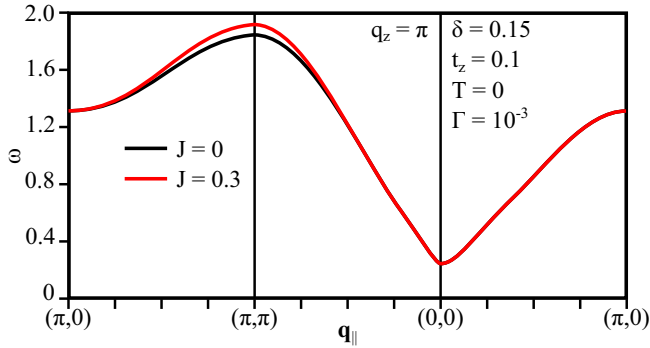


FIG. 2. Zeros of the determinant of $D_{ab}^{-1}(\mathbf{q}, \omega)$ along the symmetry axes $(\pi, 0)$ - (π, π) - $(0, 0)$ - $(\pi, 0)$ for $J = 0.3$ and $J = 0$ at $q_z = \pi$. These zeros yield collective charge excitations above the particle-hole continuum.

The zeros appear almost at the same position for both values of J . Since the 4×4 sector in Eq. (6) vanishes for $J = 0$, we can conclude that the collective peaks originate from the 2×2 sector, namely on-site charge fluctuations.

B. On-site charge susceptibility

As discussed previously [26,34], the element (1,1) of D_{ab} is related to the usual charge-charge correlation function $\chi_c(\mathbf{r}_i - \mathbf{r}_j, \tau) = \langle T_\tau n_i(\tau) n_j(0) \rangle$, which in the large- N scheme is computed in the \mathbf{q} - ω space as

$$\chi_c(\mathbf{q}, \omega) = N \left(\frac{\delta}{2} \right)^2 D_{11}(\mathbf{q}, \omega). \quad (12)$$

Thus, χ_c belongs to the 2×2 sector. The factor N on the right-hand side of the expression comes from the definition of the charge correlation function [34] in the large- N scheme, and cancels the factor $1/N$ coming from D_{ab} [see Eqs. (5), (6), and (11)], showing that χ_c is $O(1)$. The factor $(\delta/2)^2$ is due to the fact that the bosonic field δX^a must be multiplied by $\delta/2$ to become the charge fluctuations of the original Hubbard operators.

While phase separation is frequently discussed for cuprates [31,40,41], it does not occur in our model because the long-range Coulomb interaction prevents it. Recalling the frustrated phase separation mechanism [42], one might expect charge stripes instability triggered by the long-range Coulomb interaction near phase separation. This tendency, however, does not occur as studied in detail in Ref. [35].

As $\text{Im}D_{11}(\mathbf{q}, \omega)$ is already plotted in Fig. 1 for $q_z = \pi$ and was studied in detail in Ref. [29], we present results for $q_z = 8\pi/15$ in Fig. 3, which is not seen in the literature and thus may be useful for comparison between different values of q_z .

An acousticlike plasmon mode is clearly seen around $\mathbf{q}_\parallel = (0, 0)$, which has a gap of $\omega \approx 0.2$ at $\mathbf{q}_\parallel = (0, 0)$. The gap is produced by the finite interlayer hopping t_z (see Fig. 3 in Ref. [29]). This plasmon mode with a finite q_z may explain the gapped collective mode observed by RIXS [18]. A comparison between Fig. 3 and the (1,1) element in Fig. 1 demonstrates a very weak q_z dependence. However, there is a singularity at $q_z = 0$ and $\mathbf{q}_\parallel = (0, 0)$ and we obtain typical plasmons with a flat dispersion around $\mathbf{q}_\parallel = (0, 0)$ with excitation gap $\omega \approx 0.7$

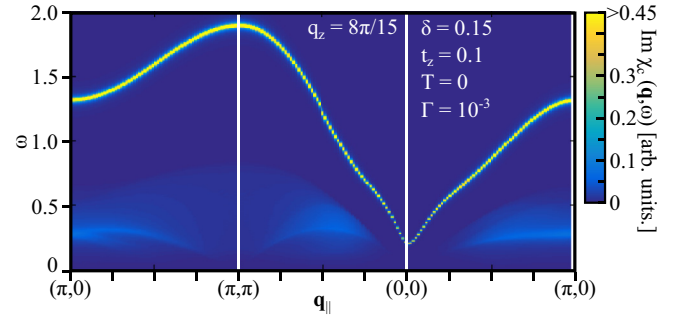


FIG. 3. \mathbf{q}_\parallel - ω map of $\text{Im}\chi_c(\mathbf{q}, \omega)$ for $q_z = 8\pi/15$. \mathbf{q}_\parallel is scanned along the symmetry axes $(\pi, 0)$ - (π, π) - $(0, 0)$ - $(\pi, 0)$.

for the present parameters at $q_z = 0$ [29] (see Fig. 8). This optical plasmon mode can be associated with the plasmons observed by optics measurements [43] and electron energy-loss spectroscopy (EELS) [44,45].

C. Bond-charge susceptibilities

The study of bond-order instabilities has an old history in the 2D t - J model [34,46–48]. However, bond-charge susceptibilities as a function of \mathbf{q}_\parallel including their dynamics have not been studied in detail. Neither are there attempts of such a study in a realistic model of cuprates such as a multilayered t - J - V model.

For $\delta = 0.15$ the homogeneous paramagnetic phase is stable down to $T = 0$ in the present model. However, there are various bond-order instabilities in the proximity to this doping that occur when an eigenvalue of the static $D_{ab}^{-1}(\mathbf{q}, 0)$ vanishes. The corresponding eigenvector determines the type of instability. (a) d -wave bond order [49], which corresponds to the freezing of the real parts of the bond variable, and the corresponding eigenvector is $V^{d \text{ bond}} = \frac{1}{\sqrt{2}}(0, 0, 1, -1, 0, 0)$, namely the bonds in the x and y directions are antiphase [see Eq. (4)]. When the propagation vector is $\mathbf{q}_\parallel = (0, 0)$, it corresponds to the d -wave Pomeranchuk instability (dPI) [50–52]. (b) s -wave bond order [49], which corresponds also to the freezing of the real parts of the bond variable, but the corresponding eigenvector is $V^{s \text{ bond}} = \frac{1}{\sqrt{2}}(0, 0, 1, 1, 0, 0)$. The bonds in the x and y directions are in phase. (c) As bond orders, eigenvectors $V = (0, 0, 1, 0, 0, 0)$ and $(0, 0, 0, 1, 0, 0)$ are also possible [26,31] and can be described by the superposition of the d -wave and s -wave bond order. (d) d -wave charge-density wave (d CDW) corresponds to the freezing of the imaginary parts of the bond variable, and the corresponding eigenvector is $V^{d \text{ CDW}} = \frac{1}{\sqrt{2}}(0, 0, 0, 0, 1, -1)$. When the modulation vector is $\mathbf{q}_\parallel = (\pi, \pi)$, it has a d -wave character and corresponds to the well-known flux phase [46–48] that describes staggered circulating currents. While charge excitations are usually studied by focusing on a certain type of charge orders, we study d - and s -wave bond orders as well as d CDW on an equal footing.

To define a bond-charge susceptibility, there may be two possibilities: (i) the projection of D_{ab} onto the corresponding eigenvectors $V^{d \text{ bond}}$, $V^{s \text{ bond}}$, and $V^{d \text{ CDW}}$, and (ii) the projection of D_{ab}^{-1} onto those eigenvectors. Although the former definition might seem natural, that definition in general contains the collective mode of the on-site charge

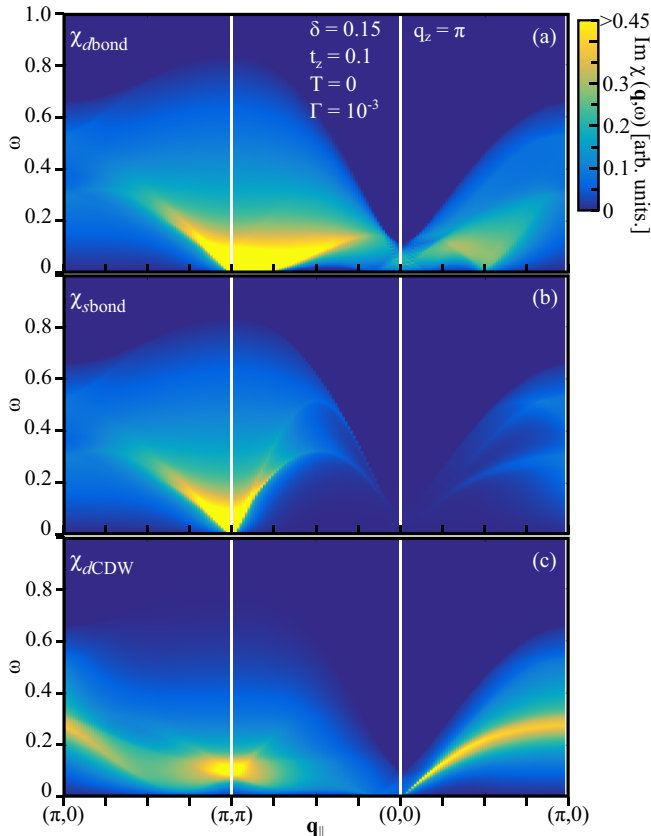


FIG. 4. \mathbf{q}_{\parallel} - ω maps of the spectral weight for (a) $\chi_{d\text{bond}}$, (b) $\chi_{s\text{bond}}$, and (c) $\chi_{d\text{CDW}}$ along the symmetry axes $(\pi, 0)$ - (π, π) - $(0, 0)$ - $(\pi, 0)$. The out-of-plane momentum is $q_z = \pi$.

fluctuations from the 2×2 sector (see Appendix B), which is thus a nongenuine feature of the bond-charge fluctuations. On the other hand, the contamination from the on-site charge excitations can be removed by adopting the latter definition. Therefore we define each bond-charge susceptibility as $\chi_{d\text{bond}}^{-1}(\mathbf{q}, \omega) = (1/N)(\delta/2)^{-2}(D_{33}^{-1} + D_{44}^{-1} - 2D_{34}^{-1})/2$, $\chi_{s\text{bond}}^{-1}(\mathbf{q}, \omega) = (1/N)(\delta/2)^{-2}(D_{33}^{-1} + D_{44}^{-1} + 2D_{34}^{-1})/2$, and $\chi_{d\text{CDW}}^{-1}(\mathbf{q}, \omega) = (1/N)(\delta/2)^{-2}(D_{55}^{-1} + D_{66}^{-1} - 2D_{56}^{-1})/2$; note that $\chi_{d\text{bond}}$ is referred to as $\chi_{d\text{PI}}$ in Ref. [26] and χ_d in Ref. [27]. The difference between $\chi_{d\text{bond}}$ and $\chi_{s\text{bond}}$ lies in the sign in front of D_{34}^{-1} . As a result, both quantities become identical for $\mathbf{q}_{\parallel} = (\pi, q_y)$ and (q_x, π) . This is easily understood. We have $h_3 = -2\Delta \sin k_x$ and $h_4 = -2\Delta \cos(k_y - \frac{q_y}{2})$ for $\mathbf{q}_{\parallel} = (\pi, q_y)$ in Eq. (7) and thus Π_{34} in Eq. (11) vanishes for $\mathbf{q}_{\parallel} = (\pi, q_y)$ and (q_x, π) , leading to $D_{34}^{-1} = 0$ there [see Eqs. (5) and (6)].

Bond-charge excitation spectra of $\chi_{d\text{bond}}(\mathbf{q}, \omega)$, $\chi_{s\text{bond}}(\mathbf{q}, \omega)$, and $\chi_{d\text{CDW}}(\mathbf{q}, \omega)$ are shown in Fig. 4 along the symmetry axes for $q_z = \pi$. Before going into the details of each excitation spectrum, we first discuss the overall features in Fig. 4. First of all, all susceptibilities exhibit positive spectral weight, although some elements of $D_{ab}(\mathbf{q}, \omega)$ contain negative spectral weight in Fig. 1. Since our choice of doping $\delta = 0.15$ is close to CO instabilities, large spectral weight is present in a relatively low-energy region $\omega \lesssim 0.2$. The spectral weight in a high-energy region is very broad and diffusive. Those features are essentially independent of q_z ,

and very similar results are obtained even in the 2D case (see Sec. III F).

$\chi_{d\text{bond}}$ shows large spectral weight at low energy around $\mathbf{q}_{\parallel} = 0.8(\pi, \pi)$. This spectral weight is associated with the leading soft mode at $\mathbf{q}_{\parallel} \approx 0.8(\pi, \pi)$, which accumulates spectral weight upon approaching the CO instability at $\delta_c = 0.129$. Along the direction $(0, 0)$ - $(\pi, 0)$ the spectrum has rather high intensity and its energy goes down toward the momentum $\mathbf{q}_{\parallel} = (0.5\pi, 0)$. This subleading mode may correspond to the CO features observed in RIXS experiments [15], as was discussed in Ref. [27]; see also Secs. III E and IV.

$\chi_{s\text{bond}}$ shows a low-energy dispersion around $\mathbf{q}_{\parallel} = (\pi, \pi)$, which is related to the proximity to the corresponding instability at $\delta_c = 0.111$. Its spectral weight disperses upwards forming a V shape and loses intensity with increasing ω . In contrast to the case of $\chi_{d\text{bond}}$, there is no CO tendency along $(0, 0)$ - $(\pi, 0)$ direction. Instead, along that direction, there is a very weak dispersive feature, which reaches $\omega \approx 0.2$ at $\mathbf{q}_{\parallel} = (0.5\pi, 0)$. This reflects a subtle structure of individual particle-hole excitations.

$\chi_{d\text{CDW}}$ exhibits large spectral weight at $\mathbf{q}_{\parallel} = (\pi, \pi)$ around $\omega = 0.1$. This energy is reduced to zero with decreasing doping towards $\delta_c = 0.093$, where the $d\text{CDW}$ instability occurs. Interestingly, there is a clear gapless dispersion along $(0, 0)$ - $(\pi, 0)$ direction and it extends up to $\omega \sim 0.3$ at $\mathbf{q}_{\parallel} = (\pi, 0)$. This is not a collective mode associated with the $d\text{CDW}$, but a peak structure of individual excitations that originates from a local minimum of the real part of the denominator of $\chi_{d\text{CDW}}$. The dispersive feature is not clearly seen along $(0, 0)$ - (π, π) direction, showing an asymmetric character of $\chi_{d\text{CDW}}$. We also see the dispersive feature in the $(\pi, 0)$ - (π, π) direction, which merges into the large spectral weight at $\mathbf{q}_{\parallel} = (\pi, \pi)$ and $\omega \approx 0.1$.

All of these bond-charge susceptibilities originate from the 4×4 sector, namely J sector in Eq. (6). Hence one might assume that a magnetic probe should be used for their detection. However, a charge probe such as RIXS can, in principle, be used for testing our results, even in the case of the $d\text{CDW}$ where most of the discussions focus on the possibility for detecting the small magnetic signal corresponding to the circulating currents.

D. Dual structure of charge-excitation spectrum

We have presented separately usual on-site charge excitations (Sec. III B) and various bond-charge excitations (Sec. III C). While it is not clear whether RIXS can detect them in a selective way or as a sum with a certain weight for each susceptibility, the full charge excitation spectrum in e-cuprates may be described by the superposition of all possible charge excitations.

Figure 5(a) shows the superposition of the spectra of χ_c , $\chi_{d\text{bond}}$, $\chi_{s\text{bond}}$, and $\chi_{d\text{CDW}}$ for $q_z = \pi$. It turns out that the total charge excitation spectrum is characterized by a dual structure: a gapped V-shaped dispersion around $\mathbf{q} = (0, 0)$ extending to a high-energy region and a continuum spectrum limited to a low-energy region typically with a scale of J ($= 0.3$). As we have shown in Secs. III A and III B, the V-shaped dispersion originates from the collective on-site charge excitations, namely a plasmon mode with a finite q_z . This mode

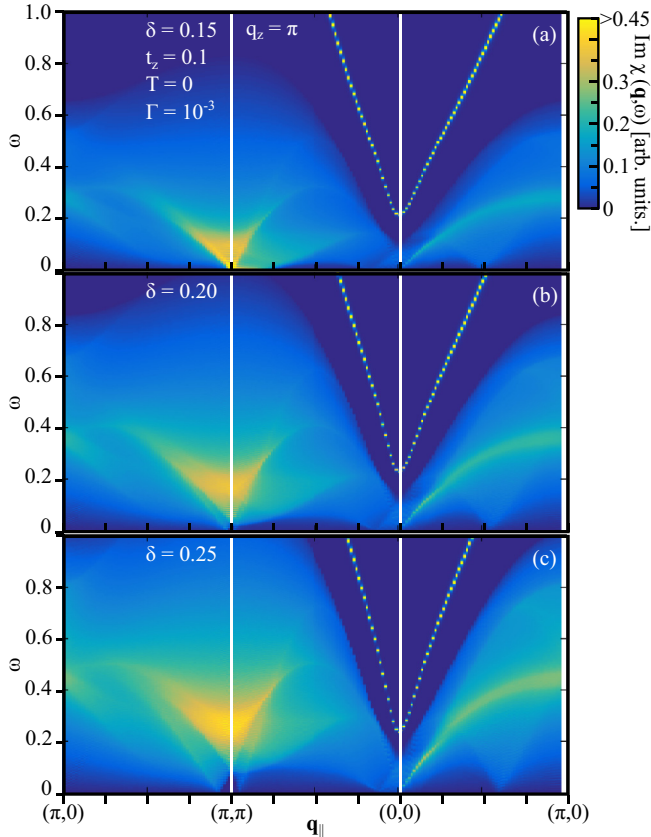


FIG. 5. \mathbf{q}_{\parallel} - ω maps of the superposition of excitation spectra of χ_c , $\chi_{d\text{bond}}$, $\chi_{s\text{bond}}$, and $\chi_{d\text{CDW}}$ along the symmetry axes $(\pi,0)$ - (π,π) - $(0,0)$ - $(\pi,0)$ for $q_z = \pi$ at three different doping rates: (a) $\delta = 0.15$, (b) $\delta = 0.20$, and (c) $\delta = 0.25$.

is controlled exclusively by the 2×2 sector in Eq. (6), with no contribution from the bond-charge excitations. On the other hand, the low-energy spectrum is the superposition of $\chi_{d\text{bond}}$, $\chi_{s\text{bond}}$, and $\chi_{d\text{CDW}}$, and the particle-hole continuum from χ_c . The former three contributions have much larger spectral weight than the last one. In Fig. 5(a) we can see a large spectral weight only around $\mathbf{q}_{\parallel} = (\pi, \pi)$ in a very low-energy region. Unfortunately RIXS cannot explore a region near $\mathbf{q}_{\parallel} = (\pi, \pi)$. The subleading CO tendency occurring at $\mathbf{q}_{\parallel} = (0.5\pi, 0)$ [see Fig. 4(a)] becomes unclear when the spectra are superimposed in Fig. 5(a), but a cusplike feature of the continuum at $\mathbf{q}_{\parallel} = (0.5\pi, 0)$ and $\omega = 0$ is barely discernible.

The dual structure should not be mixed with the usual distinction between collective excitations and the continuum spectrum. The intriguing aspect here is that their origins are completely different: the former comes from usual on-site charge fluctuations and the latter from bond-charge fluctuations. Furthermore, the continuum spectra are not composed of simply a certain type of charge order, but of various types of bond-charge fluctuations such as d -wave bond, s -wave bond, and $d\text{CDW}$.

Because of the dual structure of charge excitations, their doping dependence becomes distinct. Figures 5(b) and 5(c) show results for higher doping. The plasmon mode remains clear and nearly unchanged with increasing doping. On the other hand, the continuum spectrum typically becomes

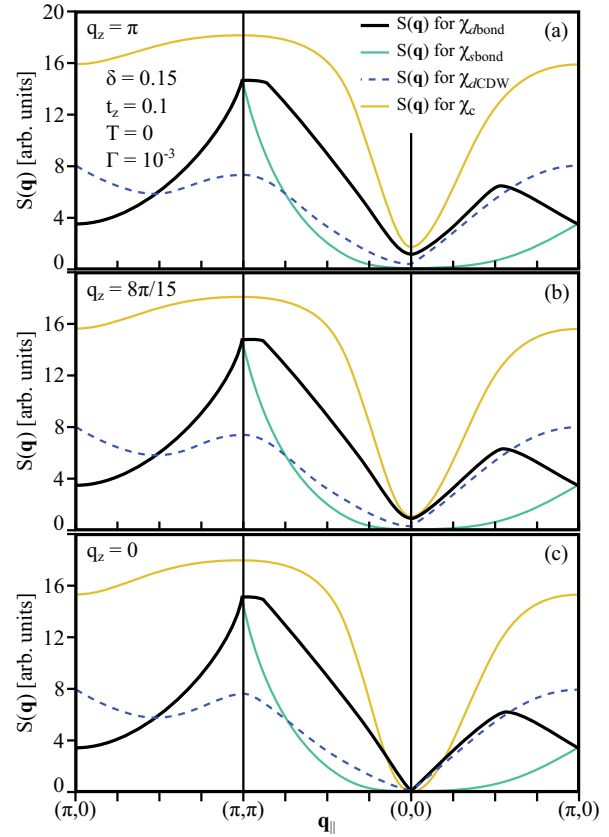


FIG. 6. $S(\mathbf{q})$ at $\delta = 0.15$ and $T = 0$ for $\chi_{d\text{bond}}$, $\chi_{s\text{bond}}$, $\chi_{d\text{CDW}}$, and χ_c along the symmetry axes $(\pi,0)$ - (π,π) - $(0,0)$ - $(\pi,0)$ for (a) $q_z = \pi$, (b) $q_z = 8\pi/15$, and (c) $q_z = 0$.

broader, but some characteristic features occur. First, the low-energy spectrum around $\mathbf{q}_{\parallel} = (\pi, \pi)$ hardens with increasing doping. This feature is easily expected because the system goes further away from the critical doping of the bond-order instability. However, unexpectedly the spectral intensity remains rather strong even at high doping. This is due to the factor $(\delta/2)^2$ in front of bond-charge susceptibility, a specific aspect of strong correlation effects in the t - J model; see also the factor $\delta/2$ in Eqs. (9) and (10) along the direction $(0,0)$ - $(\pi,0)$, a peak of the continuum becomes clearer with increasing doping. This peak originates from individual fluctuations associated with $d\text{CDW}$ as seen in Fig. 4(c).

E. ω -integrated spectral weight $S(\mathbf{q})$

While we have presented ω -resolved spectral weight, it is also interesting to study the ω -integrated spectral weight for each \mathbf{q} , namely the equal-time correlation function $S(\mathbf{q})$, because RIXS can measure it directly. For a given susceptibility χ , it is defined as

$$S(\mathbf{q}) = \frac{1}{\pi} \int_{-\infty}^{\infty} d\omega \text{Im} \chi(\mathbf{q}, \omega) [n_B(\omega) + 1], \quad (13)$$

where n_B is the Bose factor.

In Fig. 6(a) we show $S(\mathbf{q})$ for $\chi_{d\text{bond}}$, $\chi_{s\text{bond}}$, $\chi_{d\text{CDW}}$, and χ_c along the symmetry axes at $q_z = \pi$ and $\delta = 0.15$ at $T = 0$. The obtained results are easily understood by referring to Fig. 4.

The spectral weight of $\text{Im}\chi_{d\text{ bond}}^{2D}$ is very large around $\mathbf{q}_{\parallel} = (\pi, \pi)$. Thus $S(\mathbf{q})$ also exhibits a peak structure around $\mathbf{q}_{\parallel} = (\pi, \pi)$ with large weight to the side of (π, π) - $(0,0)$. Importantly, there is a subleading peak at $\mathbf{q}_{\parallel} = (0.5\pi, 0)$ along the axial direction $(0,0)$ - $(\pi, 0)$. This subleading peak is present only for d -wave bond fluctuations and originates from the low-energy spectral weight at $\mathbf{q}_{\parallel} = (0.5\pi, 0)$ in Fig. 4(a).

While a curve for s -wave bond fluctuations is not seen along the direction $(\pi, 0)$ - (π, π) in Fig. 6, $S(\mathbf{q})$ for s -wave bond fluctuations is identical to that for d -wave bond fluctuations along that direction because of symmetry (see Sec. III C). As expected from Fig. 4(b), $S(\mathbf{q})$ for s -wave bond exhibits a dominant peak at $\mathbf{q}_{\parallel} = (\pi, \pi)$. $S(\mathbf{q})$ for d CDW also exhibits a peak at $\mathbf{q}_{\parallel} = (\pi, \pi)$ much broader than that for s -wave bond. Interestingly, there is another broad peak at $\mathbf{q}_{\parallel} = (\pi, 0)$, which comes from the spectral weight associated with the dispersive feature along $(0,0)$ - $(\pi, 0)$ - $(\pi, \pi/2)$ in Fig. 4(c). For on-site charge fluctuations, $S(\mathbf{q})$ exhibits a broad dip structure around $\mathbf{q}_{\parallel} = (0,0)$. This is because the corresponding $\text{Im}\chi_c(\mathbf{q}, \omega)$ [see the $(1, 1)$ element in Figs. 1 and 3] has lower intensity around $\mathbf{q}_{\parallel} = (0,0)$ due to a small phase space of particle-hole excitations.

For completeness, we also present results for different values of q_z in Figs. 6(b) and 6(c). These results are essentially the same as Fig. 6(a) at $q_z = \pi$, indicating very weak q_z dependence of $S(\mathbf{q})$. Quantitative changes occur around $\mathbf{q}_{\parallel} = (0,0)$, where the spectral weight vanishes for all $\chi_{d\text{ bond}}^{2D}$, $\chi_{s\text{ bond}}^{2D}$, $\chi_{d\text{CDW}}^{2D}$, and χ_c at $q_z = 0$ [Fig. 6(c)], because $\text{Im}\chi$ vanishes at $\mathbf{q} = (0,0,0)$.

F. Two-dimensional t - J - V model

In the present study we have employed a layered t - J - V model with the long-range Coulomb interaction. In the literature, however, most of theoretical studies employ a 2D model. Sometimes the effect of the Coulomb interaction is also studied, but it is usually limited to the nearest-neighbor interaction such as $V(\mathbf{q}) = V(\cos q_x + \cos q_y)$. Hence it is useful to study the standard 2D t - J - V model with the nearest-neighbor Coulomb interaction and clarify the differences with previous results. We set $t_z = 0$ in Eq. (10) and replace Eq. (2) by $V(\mathbf{q}) = V(\cos q_x + \cos q_y)$ with $V = 1$, otherwise we employ the same parameters.

In Figs. 7(a)–7(c) we show results for $\chi_{d\text{ bond}}^{2D}$, $\chi_{s\text{ bond}}^{2D}$, and $\chi_{d\text{CDW}}^{2D}$, respectively. A comparison with Fig. 4 shows that the distribution of the spectral weight is very similar to each other. This means that bond-charge fluctuations are intrinsically of 2D character and are controlled by the J term of the CuO_2 plane. Although the functional form of $V(\mathbf{q})$ used in Figs. 4 and 7 is very different, such an impact is minor on bond-charge fluctuations. This is easily understood. In the bare bosonic propagator [Eq. (5)], $V(\mathbf{q})$ enters the 2×2 sector, whereas the bond field Δ the 4×4 sector. In principle, both sectors interfere with each other through Eq. (6). However, our actual calculations in Secs. III A–III D have showed that both sectors are essentially decoupled. In addition, we find that the critical doping and critical temperatures of bond orders in the 2D model [31] are almost the same as those obtained in the layered model. This is another evidence that bond-charge fluctuations are controlled by the J term in the 2D plane.

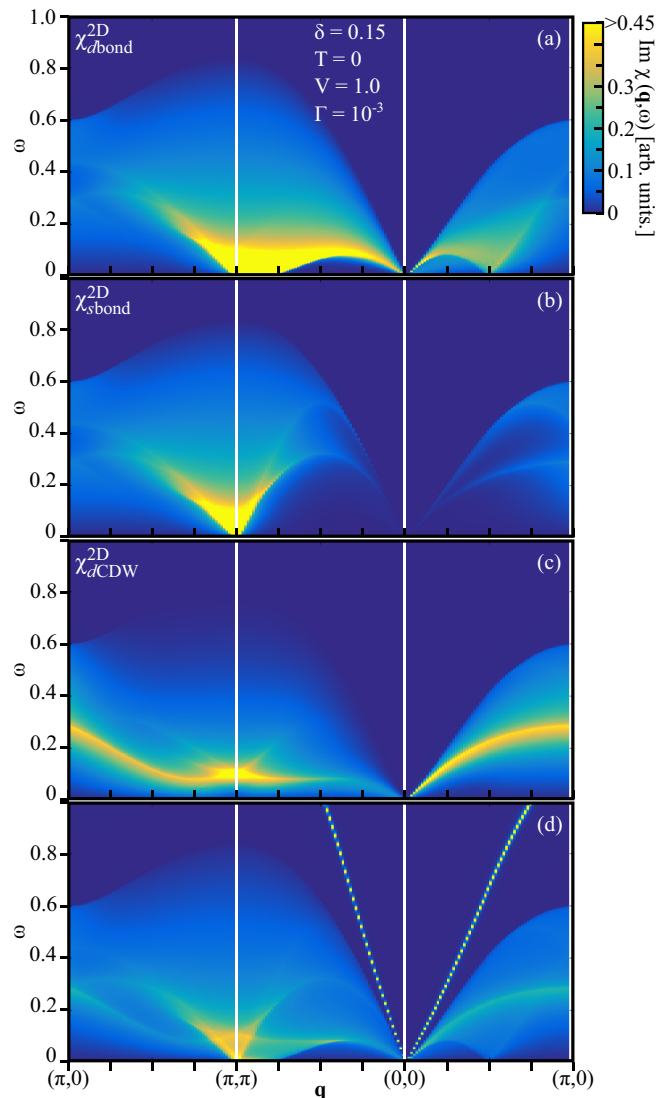


FIG. 7. Charge excitation spectra for (a) $\chi_{d\text{ bond}}^{2D}$, (b) $\chi_{s\text{ bond}}^{2D}$, and (c) $\chi_{d\text{CDW}}^{2D}$ in the 2D t - J - V model along the symmetry axes $(\pi, 0)$ - (π, π) - $(0, 0)$ - $(\pi, 0)$. (d) Superposition of the spectra of χ_c^{2D} , $\chi_{d\text{ bond}}^{2D}$, $\chi_{s\text{ bond}}^{2D}$, and $\chi_{d\text{CDW}}^{2D}$.

Usual on-site charge excitations (χ_c^{2D}) were already computed in Fig. 1(c) in Ref. [35]. Instead of reproducing such a result, we show the superposition of $\text{Im}\chi_c^{2D}$, $\text{Im}\chi_{d\text{ bond}}^{2D}$, $\text{Im}\chi_{s\text{ bond}}^{2D}$, and $\text{Im}\chi_{d\text{CDW}}^{2D}$ in Fig. 7(d). Similar to the case of Fig. 5, the continuum spectra come mainly from bond-charge fluctuations. The major contribution from the on-site charge excitations is a gapless linear dispersion around $\mathbf{q} = (0, 0)$ above the continuum. This is not a plasmon mode, but a zero-sound mode due to the short-range Coulomb interaction $V(\mathbf{q})$. Hence the spectrum of $\text{Im}\chi_c^{2D}$ is very different from Sec. III B, where q_z is finite and we have obtained plasmon excitations with an energy gap which is scaled by interlayer hopping t_z (see Fig. 3 in Ref. [29]). Hence the functional form of $V(\mathbf{q})$ and dimensionality are crucial to the collective mode above the particle-hole continuum.

Since the form of $V(\mathbf{q})$ is important to on-site charge excitations, it is insightful to mention also results in the

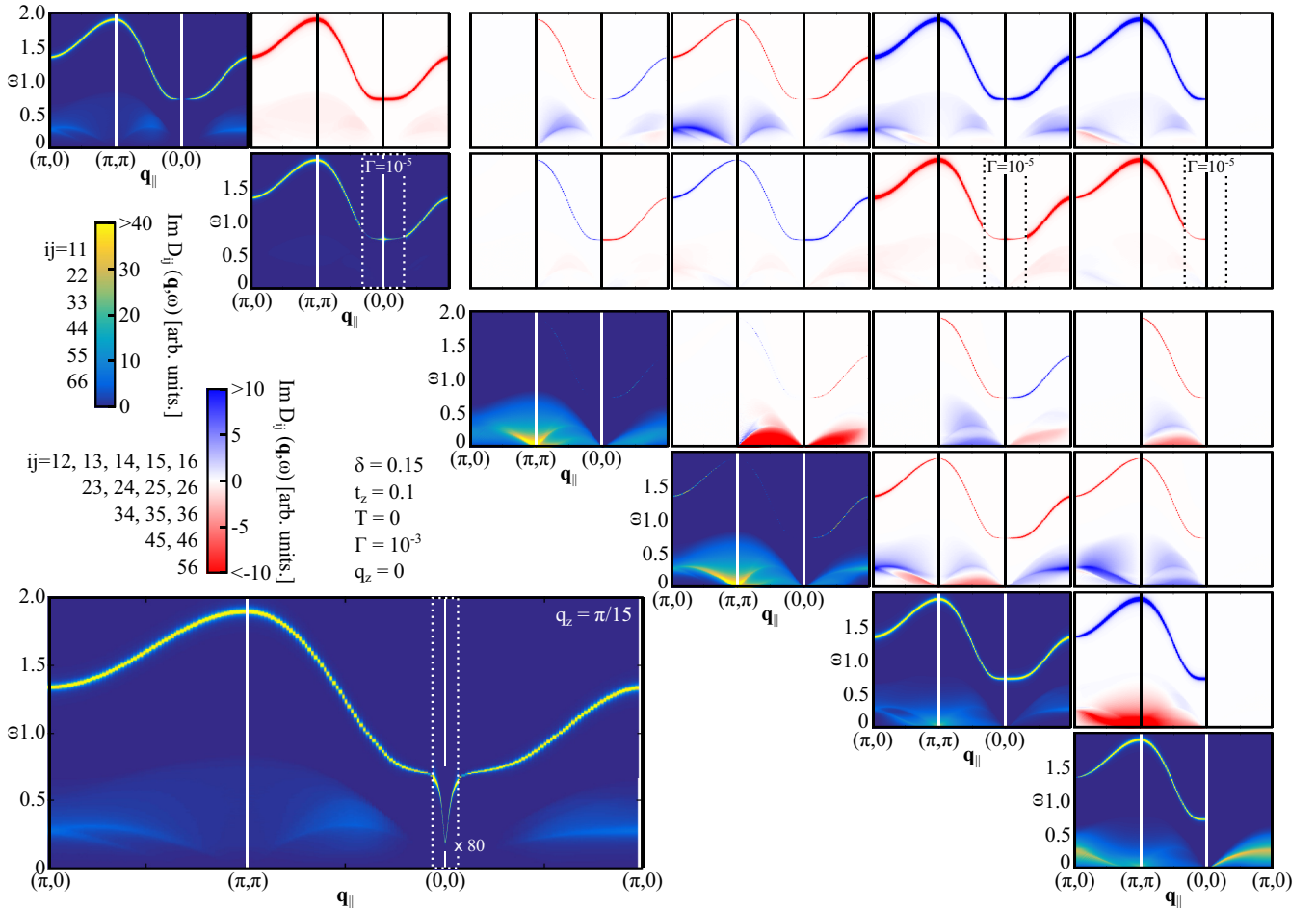


FIG. 8. \mathbf{q}_{\parallel} - ω maps of each element of $\text{Im}D_{ab}(\mathbf{q}, \omega)$ along the symmetry axes $(\pi, 0)$ - (π, π) - $(0, 0)$ - $(\pi, 0)$. The out-of-plane momentum is $q_z = 0$. The elements are placed in a 6×6 matrix form and only the upper triangular matrix is shown because $D_{ab}(\mathbf{q}, \omega)$ is symmetric. To clarify each sector of 2×2 , 4×4 , and 2×4 , a small space is inserted between each sector. In the elements (2,2), (2,5), and (2,6), we choose a smaller $\Gamma = 10^{-5}$ to increase the accuracy when computing near $\mathbf{q}_{\parallel} = (0, 0)$. The inset (bottom left) is the element (1,1) at $q_z = \pi/15$. To make a better contrast, the spectral intensity around $\mathbf{q}_{\parallel} = (0, 0)$ is multiplied by 80 and the vertical axis line at $\mathbf{q}_{\parallel} = (0, 0)$ is broken between $\omega = 0.1$ and 0.75 .

presence of the long-range Coulomb interaction. Typically we may have two cases. (i) The 2D t - J model with the three-dimensional long-range Coulomb interaction [Eq. (2)]. While for $q_z = 0$ the usual optical plasmon mode is realized around $\mathbf{q}_{\parallel} = (0, 0)$ as seen in the (1,1) element in Fig. 8, the plasmon energy drops to zero once q_z becomes finite and a gapless acoustic plasmon mode is realized. This corresponds to the present model with $t_z = 0$ (see Fig. 3 in Ref. [29]) and to the case of Ref. [53]. (ii) The 2D t - J model with the 2D long-range Coulomb interaction, i.e., $V(\mathbf{q}) \sim 1/q$. In this case, we obtain a gapless plasmon dispersion $\omega(\mathbf{q}) \sim \sqrt{q}$ as is well known [54].

IV. DISCUSSIONS

We have shown that the charge excitation spectrum in the t - J model exhibits a dual structure. One is usual on-site charge fluctuations, which are realized as plasmons in a relatively high-energy region ($\omega \gtrsim 0.3$) above the particle-hole

continuum. The other is bond-charge fluctuations driven by the exchange interaction J and can lead to CO phenomena. Its spectral weight appears in a low-energy region, typically less than $J (= 0.3)$. Since the lattice site in the present model corresponds to a Cu atom in the CuO_2 plane, we reasonably interpret that the on-site charge fluctuations correspond to fluctuations on the Cu sites and bond-charge fluctuations, i.e., fluctuations between the nearest-neighbor Cu sites correspond to charge fluctuations at the O sites. This interpretation is actually supported by explicit calculations [23] in the three-band Hubbard model where both Cu and O sites are included. Hence our theory suggests that the high-energy charge fluctuations consist mainly of the on-site charge fluctuations at the Cu sites, and low-energy charge excitations originate mainly from the O sites.

The high-energy charge excitations are captured correctly only when both the interlayer coupling and the long-range Coulomb interaction are taken into account. The 2D t - J model studied frequently cannot capture the correct high-energy

features even if the long-range Coulomb repulsion is included. On the other hand, the low-energy features can be well described by the 2D t - J model and the long-range Coulomb interaction is unimportant. The distinction between low- and high-energy regimes, which we call a dual structure, is crucial to understand the complicated charge excitations in cuprates. Theoretically this dual structure means, in the language of the 6×6 bosonic propagator D_{ab} [Eq. (6)], that the 2×2 sector and the 4×4 sector or J sector are essentially decoupled; the former controls on-site charge fluctuations and the latter bond-charge fluctuations.

The experimental indications of the underlying dual structure of charge excitation spectrum are actually obtained by different methods. RIXS revealed the quasilinear dispersive mode near $\mathbf{q}_{\parallel} = (0,0)$ [18,19]). Since the value of q_z is finite in RIXS, this mode is interpreted as an acousticlike plasmon mode from the usual on-site charge excitations [29]. On the other hand, charge excitations were also reported by RXS [15,16]. RXS measures ω -integrated spectral weight for each \mathbf{q} [Eq. (13)] and reported a short-range charge order with $\mathbf{q}_{\parallel} \approx (0.48\pi, 0)$ in e-cuprates [15,16]. This signal was discussed as originating from $\chi_{d \text{ bond}}$ [27], namely from the low-energy charge fluctuations driven by the J term. While the 2D t - J model was employed in Ref. [27], the present work (Fig. 6) indeed finds a peak near $\mathbf{q}_{\parallel} = (0.5\pi, 0)$ only in the d -wave bond-charge susceptibility, confirming that the conclusions obtained in Ref. [27] are valid also in the layered t - J - V model. Therefore the short-range charge-order observed in e-cuprates [15,16] can be a short-range d -wave bond order.

An additional implication from the present work is that there can be a stronger tendency of bond-charge orders near $\mathbf{q}_{\parallel} = (\pi, \pi)$ as seen in Fig. 4. Interestingly not only $\chi_{d \text{ bond}}$ but also $\chi_{s \text{ bond}}$ and $\chi_{d \text{ CDW}}$ contribute to the low-energy charge fluctuations around $\mathbf{q}_{\parallel} = (\pi, \pi)$. Unfortunately this possibility cannot be tested by resonant x-ray measurement because such a momentum region is out of its range. Further experimental techniques are necessary for detecting them. Far away from (π, π) , on the other hand, $\chi_{d \text{ bond}}$ and $\chi_{d \text{ CDW}}$ exhibit a dispersive feature along $(0,0)$ - $(\pi, 0)$ direction [see Figs. 4(a), 4(c), 7(a), and 7(c)], which may be tested by RIXS.

As clarified in Ref. [31], the tendency to CO instabilities in e-cuprates is very different from that in h-cuprates. Hence we expect strong particle-hole asymmetry of bond-charge fluctuations driven by the exchange interaction J . The present results of bond-charge excitation spectra may not be applied straightforwardly to h-cuprates, but provide a good basis to understand complicated charge excitation spectra. On the other hand, the usual on-site charge excitations, namely plasmon excitations, are general features and we expect a similar mode also in h-cuprates. In fact, such a mode with a finite q_z seems to be observed in RIXS in Ref. [30]. However, the authors of Ref. [30] interpreted them as individual on-site charge excitations, not as plasmons. In the present work, the individual on-site charge excitations, namely the continuum excitations, are weak as seen in the low-energy region in Fig. 1. Moreover, its spectral weight is even weaker than that of bond-charge excitations. Hence

plasmons seem a more natural interpretation of the data of Ref. [30].

While q_z is finite in RIXS, the plasmon mode with $q_z = 0$ can be detected in EELS [44,45]. EELS observes the loss function, namely $\text{Im}(\frac{1}{\epsilon(\mathbf{q}, \omega)}) \propto V(\mathbf{q}) \text{Im}\chi_c(\mathbf{q}, \omega)$. The spectral weight of $\text{Im}\chi_c(\mathbf{q}, \omega)$ is proportional to q^2 at the plasmon energy and thus vanishes at $\mathbf{q} = (0,0,0)$ [see Fig. 6(c) and the (1,1) element in Fig. 8]. However, the loss function becomes finite at $\mathbf{q} = (0,0,0)$ because of the singularity of the long-range Coulomb interaction in the long-wavelength limit, namely $V(\mathbf{q}) \propto q^{-2}$.

V. CONCLUSIONS

The layered t - J - V model treated in a large- N expansion shows a dual structure of charge excitation spectra. (i) In a low-energy region, the spectral weight originates mainly from various types of bond-charge fluctuations with internal symmetry, for example, $\cos k_x - \cos k_y$. These bond-charge fluctuations are triggered by the exchange term J , and can lead to the charge order phenomena. The low-energy spectral weight is essentially independent of the out-of-plane momentum q_z . (ii) In the high-energy region, the spectral weight is dominated by usual on-site charge fluctuations and is characterized by a plasmon mode with a minimal excitation gap at $\mathbf{q}_{\parallel} = (0,0)$. The dispersion around $\mathbf{q}_{\parallel} = (0,0)$ is quasilinear for a finite q_z , whereas it is flat for $q_z = 0$ similar to usual optical plasmons. The dual structure of charge excitation spectra that we have elucidated in the present paper will serve to disentangle major charge excitations from complicated spectra of RIXS data.

ACKNOWLEDGMENTS

The authors thank K. Ishii and T. Tohyama for very fruitful discussions about RIXS. H.Y. acknowledges support by JSPS KAKENHI Grant No. 15K05189. A.G. acknowledges the Japan Society for the Promotion of Science for a Short-term Invitational Fellowship program (S17027) under which this work was completed.

APPENDIX A: ELEMENTS OF $\text{Im}D_{ab}(\mathbf{q}, \omega)$ AT DIFFERENT q_z

As we have mentioned in Sec. III A, each element of $\text{Im}D_{ab}(\mathbf{q}, \omega)$ exhibits essentially the same result for different values of q_z except for the collective mode around $\mathbf{q}_{\parallel} = (0,0)$. To demonstrate such a statement, we present results for $q_z = 0$ in Fig. 8. A comparison with the result for $q_z = \pi$ (Fig. 1) shows that the continuum spectra are in fact essentially the same and the crucial difference is recognized in the plasmon mode around $\mathbf{q}_{\parallel} = (0,0)$. The plasmons feature a flat dispersion around $\mathbf{q}_{\parallel} = (0,0)$ for $q_z = 0$ and a quasilinear dispersion for $q_z = \pi$. The flat dispersion, however, appears only at $q_z = 0$ and its gap suddenly drops from $\omega \approx 0.7$ to $\omega \approx 0.2$ once q_z becomes finite, yielding a sharp V-shaped dispersion as shown in the inset of Fig. 8. With increasing q_z ,

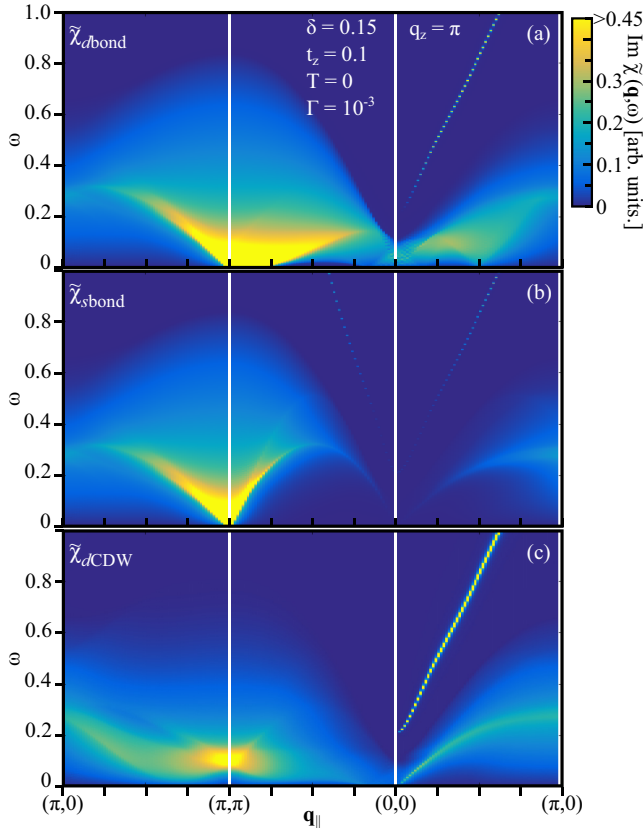


FIG. 9. \mathbf{q}_{\parallel} - ω maps of $\text{Im}\tilde{\chi}_{d\text{bond}}(\mathbf{q}, \omega)$, $\text{Im}\tilde{\chi}_{s\text{bond}}(\mathbf{q}, \omega)$, and $\text{Im}\tilde{\chi}_{d\text{CDW}}(\mathbf{q}, \omega)$ along the symmetry axes $(\pi, 0)$ - (π, π) - $(0, 0)$ - $(\pi, 0)$; the out-of-plane momentum is $q_z = \pi$.

the energy gap stays at $\omega \approx 0.2$ and the slope of the V-shaped dispersion decreases. For $q_z \gtrsim 0.4\pi$, the V-shape dispersion becomes almost the same as that at $q_z = \pi$, which was clearly shown in Fig. 2 in Ref. [29].

APPENDIX B: ALTERNATIVE DEFINITION OF BOND-CHARGE SUSCEPTIBILITY

As we have discussed in Sec. III C, each bond-charge susceptibility may also be defined by the projection of D_{ab} , not D_{ab}^{-1} , onto the corresponding eigenvectors $V^{d\text{bond}}$, $V^{s\text{bond}}$, and $V^{d\text{CDW}}$. That is, $\tilde{\chi}_{d\text{bond}}(\mathbf{q}, \omega) = N(\delta/2)^2(D_{33} + D_{44} - 2D_{34})/2$, $\tilde{\chi}_{s\text{bond}}(\mathbf{q}, \omega) = N(\delta/2)^2(D_{33} + D_{44} + 2D_{34})/2$, and $\tilde{\chi}_{d\text{CDW}}(\mathbf{q}, \omega) = N(\delta/2)^2(D_{55} + D_{66} - 2D_{56})/2$. Their spectra, namely the imaginary part of each susceptibility, are shown in Fig. 9. The continuum spectrum is essentially the same as that shown in Fig. 4 in Sec. III C. A crucial difference is the presence of collective excitations from the on-site charge fluctuations, which remain strong along $(0, 0)$ - $(\pi, 0)$ direction especially for $\tilde{\chi}_{d\text{CDW}}$. Because of symmetry there is no collective excitations along $(0, 0)$ - (π, π) direction for $\tilde{\chi}_{d\text{CDW}}$ and $\tilde{\chi}_{d\text{bond}}$. Along $(\pi, 0)$ - (π, π) direction the energy of the collective excitation becomes larger than 1 ($= t$). The presence of these collective excitations may be apparent from Fig. 1 where all elements of D_{ab} , in principle, contain the collective on-site charge excitations above the continuum spectrum as we have discussed in Sec. III A. Thus $\tilde{\chi}_{d\text{bond}}$, $\tilde{\chi}_{s\text{bond}}$, and $\tilde{\chi}_{d\text{CDW}}$ necessarily have such contamination.

- [1] T. Wu, H. Mayaffre, S. Krämer, M. Horvatić, C. Berthier, W. N. Hardy, R. Liang, D. A. Bonn, and M.-H. Julien, *Nature (London)* **477**, 191 (2011).
- [2] G. Ghiringhelli, M. LeTacon, M. Minola, S. Blanco-Canosa, C. Mazzoli, N. B. Brookes, G. M. D. Luca, A. Frano, D. G. Hawthorn, F. He, T. Loew, M. M. Sala, D. C. Peets, M. Salluzzo, E. Schierle, R. Sutarto, G. A. Sawatzky, E. Weschke, B. Keimer, and L. Braicovich, *Science* **337**, 821 (2012).
- [3] J. Chang, E. Blackburn, A. T. Holmes, N. B. Christensen, J. Larsen, J. Mesot, R. Liang, D. A. Bonn, W. N. Hardy, A. Watenphul, E. M. F. M. v. Zimmermann, and S. M. Hayden, *Nat. Phys.* **8**, 871 (2012).
- [4] A. J. Achkar, R. Sutarto, X. Mao, F. He, A. Frano, S. Blanco-Canosa, M. LeTacon, G. Ghiringhelli, L. Braicovich, M. Minola, M. Moretti Sala, C. Mazzoli, R. Liang, D. A. Bonn, W. N. Hardy, B. Keimer, G. A. Sawatzky, and D. G. Hawthorn, *Phys. Rev. Lett.* **109**, 167001 (2012).
- [5] E. Blackburn, J. Chang, M. Hücker, A. T. Holmes, N. B. Christensen, R. Liang, D. A. Bonn, W. N. Hardy, U. Rütt, O. Gutowski, M. v. Zimmermann, E. M. Forgan, and S. M. Hayden, *Phys. Rev. Lett.* **110**, 137004 (2013).
- [6] D. LeBoeuf, S. Krämer, W. N. Hardy, R. Liang, D. A. Bonn, and C. Proust, *Nat. Phys.* **9**, 79 (2013).
- [7] S. Blanco-Canosa, A. Frano, E. Schierle, J. Porras, T. Loew, M. Minola, M. Bluschke, E. Weschke, B. Keimer, and M. LeTacon, *Phys. Rev. B* **90**, 054513 (2014).
- [8] R. Comin, A. Frano, M. M. Yee, Y. Yoshida, H. Eisaki, E. Schierle, E. Weschke, R. Sutarto, F. He, A. Soumyanarayanan, Y. He, M. LeTacon, I. S. Elfimov, J. E. Hoffman, G. A. Sawatzky, B. Keimer, and A. Damascelli, *Science* **343**, 390 (2014).
- [9] E. H. da Silva Neto, P. Aynajian, A. Frano, R. Comin, E. Schierle, E. Weschke, A. Gyenis, J. Wen, J. Schneeloch, Z. Xu, S. Ono, G. Gu, M. LeTacon, and A. Yazdani, *Science* **343**, 393 (2014).
- [10] M. Hashimoto, G. Ghiringhelli, W.-S. Lee, G. Dellea, A. Amorese, C. Mazzoli, K. Kummer, N. B. Brookes, B. Moritz, Y. Yoshida, H. Eisaki, Z. Hussain, T. P. Devereaux, Z.-X. Shen, and L. Braicovich, *Phys. Rev. B* **89**, 220511 (2014).
- [11] W. Tabis, Y. Li, M. LeTacon, L. Braicovich, A. Kreyssig, M. Minola, G. Dellea, E. Weschke, M. J. Veit, M. Ramazanoglu, A. I. Goldman, T. Schmitt, G. Ghiringhelli, N. Barišić, M. K. Chan, C. J. Dorow, G. Yu, X. Zhao, B. Keimer, and M. Greven, *Nat. Commun.* **5**, 5875 (2014).
- [12] S. Gerber, H. Jang, H. Nojiri, S. Matsuzawa, H. Yasumura, D. A. Bonn, R. Liang, W. N. Hardy, Z. Islam, A. Mehta, S. Song, M. Sikorski, D. Stefanescu, Y. Feng, S. A. Kivelson, T. P. Devereaux, Z.-X. Shen, C.-C. Kao, W.-S. Lee, D. Zhu, and J.-S. Lee, *Science* **350**, 949 (2015).
- [13] Y. Y. Peng, M. Salluzzo, X. Sun, A. Ponti, D. Betto, A. M. Ferretti, F. Fumagalli, K. Kummer, M. LeTacon, X. J. Zhou, N. B. Brookes, L. Braicovich, and G. Ghiringhelli, *Phys. Rev. B* **94**, 184511 (2016).

- [14] W. Tabis, B. Yu, I. Bialo, M. Bluschke, T. Kolodziej, A. Kozłowski, Y. Tang, E. Weschke, B. Vignolle, M. Hepting, H. Gretarsson, R. Sutarto, F. He, M. LeTacon, N. Barisik, G. Yu, and M. Greve, *Phys. Rev. B* **96**, 134510 (2017).
- [15] E. H. da Silva Neto, R. Comin, F. He, R. Sutarto, Y. Jiang, R. L. Greene, G. A. Sawatzky, and A. Damascelli, *Science* **347**, 282 (2015).
- [16] E. H. da Silva Neto, B. Yu, M. Minola, R. Sutarto, E. Schierle, F. Boschini, M. Zonno, M. Bluschke, J. Higgins, Y. Li, G. Yu, E. Weschke, F. He, M. LeTacon, R. L. Greene, M. Greven, G. A. Sawatzky, B. Keimer, and A. Damascelli, *Sci. Adv.* **2**, 1600782 (2016).
- [17] R. G. N. Armitage and P. Fournier, *Rev. Mod. Phys.* **82**, 2421 (2010).
- [18] W. S. Lee, J. J. Lee, E. A. Nowadnick, S. Gerber, W. Tabis, S. W. Huang, V. N. Strocov, E. M. Motoyama, G. Yu, B. Moritz, H. Y. Huang, R. P. Wang, Y. B. Huang, W. B. Wu, C. T. Chen, D. J. Huang, M. Greven, T. Schmitt, Z. X. Shen, and T. P. Devereaux, *Nat. Phys.* **10**, 883 (2014).
- [19] K. Ishii, M. Fujita, T. Sasaki, M. Minola, G. Dellea, C. Mazzoli, K. Kummer, G. Ghiringhelli, L. Braicovich, T. Tohyama, K. Tsutsumi, K. Sato, R. Kajimoto, K. Ikeuchi, K. Yamada, M. Yoshida, M. Kurooka, and J. Mizuki, *Nat. Commun.* **5**, 3714 (2014).
- [20] A. Allais, J. Bauer, and S. Sachdev, *Phys. Rev. B* **90**, 155114 (2014).
- [21] H. Meier, C. Pépin, M. Eilenkel, and K. B. Efetov, *Phys. Rev. B* **89**, 195115 (2014).
- [22] Y. Wang and A. Chubukov, *Phys. Rev. B* **90**, 035149 (2014).
- [23] W. Atkinson, A. Kampf, and S. Bulut, *New J. Phys.* **17**, 013025 (2015).
- [24] Y. Yamakawa and H. Kontani, *Phys. Rev. Lett.* **114**, 257001 (2015).
- [25] V. Mishra and M. R. Norman, *Phys. Rev. B* **92**, 060507 (2015).
- [26] M. Bejas, A. Greco, and H. Yamase, *Phys. Rev. B* **86**, 224509 (2012).
- [27] H. Yamase, M. Bejas, and A. Greco, *Europhys. Lett.* **111**, 57005 (2015).
- [28] Z.-X. Li, F. Wang, H. Yao, and D.-H. Lee, *Phys. Rev. B* **95**, 214505 (2017).
- [29] A. Greco, H. Yamase, and M. Bejas, *Phys. Rev. B* **94**, 075139 (2016).
- [30] K. Ishii, T. Tohyama, S. Asano, K. Sato, M. Fujita, S. Wakimoto, K. Tustsui, S. Sota, J. Miyawaki, H. Niwa, Y. Harada, J. Pellicciari, Y. Huang, T. Schmitt, Y. Yamamoto, and J. Mizuki, *Phys. Rev. B* **96**, 115148 (2017).
- [31] M. Bejas, A. Greco, and H. Yamase, *New J. Phys.* **16**, 123002 (2014).
- [32] T. Thio, T. R. Thurston, N. W. Preyer, P. J. Picone, M. A. Kastner, H. P. Jenssen, D. R. Gabbe, C. Y. Chen, R. J. Birgeneau, and A. Aharony, *Phys. Rev. B* **38**, 905 (1988).
- [33] F. Becca, M. Tarquini, M. Grilli, and C. DiCastro, *Phys. Rev. B* **54**, 12443 (1996).
- [34] A. Foussats and A. Greco, *Phys. Rev. B* **70**, 205123 (2004).
- [35] A. Greco, H. Yamase, and M. Bejas, *J. Phys. Soc. Jpn.* **86**, 034706 (2017).
- [36] F. C. Zhang and T. M. Rice, *Phys. Rev. B* **37**, 3759 (1988).
- [37] M. S. Hybertsen, E. B. Stechel, M. Schluter, and D. R. Jennison, *Phys. Rev. B* **41**, 11068 (1990).
- [38] Although CuO_2 planes shift by $(\frac{1}{2}, \frac{1}{2}, \frac{1}{2})$ in $\text{Nd}_{2-x}\text{Ce}_x\text{CuO}_4$, we model the actual system by neglecting such a shift for simplicity. Our interlayer distance d is thus given by a half of the c -axis lattice constant.
- [39] T. Timusk and D. Tanner, *Infrared Properties of High-Tc Superconductors* (World Scientific, Singapore, 1989).
- [40] G. B. Martins, J. C. Xavier, L. Arrachea, and E. Dagotto, *Phys. Rev. B* **64**, 180513(R) (2001).
- [41] A. Macridin, M. Jarrell, and T. Maier, *Phys. Rev. B* **74**, 085104 (2006).
- [42] V. J. Emery and S. A. Kivelson, *Physica C* **209**, 597 (1993).
- [43] E. J. Singley, D. N. Basov, K. Kurahashi, T. Uefuji, and K. Yamada, *Phys. Rev. B* **64**, 224503 (2001).
- [44] N. Nücker, H. Romberg, S. Nakai, B. Scheerer, J. Fink, Y. F. Yan, and Z. X. Zhao, *Phys. Rev. B* **39**, 379 (1989).
- [45] H. Romberg, N. Nücker, J. Fink, T. Wolf, X. X. Xi, B. Koch, H. P. Geserich, M. Dürzler, W. Assmus, and B. Gegenheimer, *Z. Phys. B* **78**, 367 (1990).
- [46] I. Affleck and J. B. Marston, *Phys. Rev. B* **37**, 3774 (1988).
- [47] D. C. Morse and T. C. Lubensky, *Phys. Rev. B* **43**, 10436 (1991).
- [48] E. Cappelluti and R. Zeyher, *Phys. Rev. B* **59**, 6475 (1999).
- [49] Bond orders are referred to as bond-order-phase (BOP) in literature [26,31], where d -wave and s -wave bond orders correspond to $\text{BOP}_{x\bar{y}}$ and BOP_{xy} , respectively.
- [50] H. Yamase and H. Kohno, *J. Phys. Soc. Jpn.* **69**, 332 (2000).
- [51] H. Yamase and H. Kohno, *J. Phys. Soc. Jpn.* **69**, 2151 (2000).
- [52] C. J. Halboth and W. Metzner, *Phys. Rev. Lett.* **85**, 5162 (2000).
- [53] P. Prelovšek and P. Horsch, *Phys. Rev. B* **60**, R3735(R) (1999).
- [54] G. F. Giuliani and G. Vignale, *Quantum Theory of the Electron Liquid* (Cambridge University Press, Cambridge, 2005).